

Dynamic Mortality Risk Predictions in Pediatric Critical Care Using Recurrent Neural Networks

Melissa Aczon[†], David Ledbetter*, Long Van Ho, Alec Gunny,
Alysia Flynn, Jon Williams, Randall Wetzel

The Laura P. and Leland K. Whittier Virtual Pediatric Intensive Care Unit
Children’s Hospital Los Angeles

Abstract

Viewing the trajectory of a patient as a dynamical system, a recurrent neural network was developed to learn the course of patient encounters in the Pediatric Intensive Care Unit (PICU) of a major tertiary care center. Data extracted from Electronic Medical Records (EMR) of about 12000 patients who were admitted to the PICU over a period of more than 10 years were leveraged. The RNN model ingests a sequence of measurements which include physiologic observations, laboratory results, administered drugs and interventions, and generates temporally dynamic predictions for in-ICU mortality at user-specified times. The RNN’s ICU mortality predictions offer significant improvements over those from two clinically-used scores and static machine learning algorithms.

1. Introduction

1.1 Background on severity and mortality scores

Numerous severity of illness (SOI) and mortality scoring systems have been developed over the past three decades [Le Gall (2005); Strand and Flaatten (2008)]. Two of the earliest and commonly used scores are Acute Physiology and Chronic Health Evaluation (APACHE II), [Knaus et al. (1985)] and Simplified Acute Physiology Score (SAPS) [Le Gall et al. (1984)], both of which rely on routine physiologic measurements and the deviations of those measurements from expert-defined *normal* values. In pediatric critical care, the Pediatric Risk of Mortality (PRISM), [Pollack et al. (1988)] score and Pediatric Index of Mortality (PIM), [Shann et al. (1997)] were developed. Both leverage physiologic data, with PIM incorporating into its calculations additional information such as pre-ICU procedures and in-ICU ventilation data from the first hour. Larger databases led to refinements of these systems; for some examples, see APACHE III in Knaus et al. (1991); SAPS 3 in Moreno et al. (2005); PRISM 3 in Pollack et al. (1996); PRISM 4 in Pollack et al. (2016); PIM 2 in Slater et al. (2003); PIM 3 in Straney et al. (2013). Pollack (2016) makes a distinction between scoring for severity of illness or predicting mortality. Regardless of this distinction, however, the effectiveness of these models are measured via their ability to discriminate between surviving and non-surviving patients.

[†]Correspondence: {maczon, dledbetter, loho, agunny, aflynn, jonwilliams, rwetzel}@chla.usc.edu

*The first two authors contributed equally to this work.

1.2 EMR and advanced computing methods

The adoption of Electronic Medical Records (EMR) has enabled ready access to more variables and more patients. In response to this ever-growing amount of data, machine learning techniques increasingly have been used to develop models which forecast patient condition. The Gaussian process-based scores in Ghassemi et al. (2015) and Alaa et al. (2016) leverage time-series measurements instead of static values from a fixed time window of the systems described earlier. Towards personalized scoring, the latter attempts to account for heterogeneity by discovering, via unsupervised learning, some number of *classes* in the population, then learns the parameters that govern each class. The Rothman index [Rothman et al. (2013)] also offers continuously updated scores but still generates predictions using a static snapshot.

The use of neural networks in ICU applications actually goes back more than 20 years, as reviewed in Hanson III and Marshall (2001). In general those studies were relatively small in scale (hundreds of patients). Since then, two primary factors have changed the landscape. First, larger datasets containing tens of thousands of patients with millions of measurements are now available. Second, computing hardware advances in the last decade, particularly Graphics Processing Units (GPUs), have enabled larger, deeper networks to be trained. These more sophisticated networks have demonstrated remarkable success in wide-ranging applications such as computer vision [Krizhevsky et al. (2012); He et al. (2015)], speech recognition [Hinton et al. (2012)], and natural language processing [Mesnil et al. (2015)].

1.3 Summary of RNN-based mortality model/framework

Recurrent Neural Networks (RNN) were designed to process sequential data. A key feature is a *feedback loop* which allows integration of information from previous steps with newly acquired data. Thus, they provide an elegant infrastructure to process ever-evolving streams of clinical data. Figure 1 gives a high-level illustration of data ingestion and prediction with a RNN, and Section 3.1 will describe the mathematical formulation. Each input vector (x) contains clinical measurements (e.g. physiology and medications). The infrastructure also allows the user to specify how long into the future predictions are for. Each output vector (y) contains forecasts such as mortality risk at the specified future time. This work focused on predicting in-ICU mortality of pediatric patients. Hospital mortality is used because it is an objective function to assess performance despite its inability to capture more subjective components of care such as quality of survival [Knaus et al. (1985)]. Also, the sequential nature of the RNN’s mortality risk predictions provides a dynamic tracking of patient condition.

2. Data and pre-processing

We leveraged anonymized EMR from the PICU at Children’s Hospital Los Angeles between December 2002 and March 2016. The data for each patient included static information such as demographics, diagnoses, and disposition (alive or not) at the end of the ICU encounter. An encounter is defined as a contiguous admission into the PICU. Each encounter contained irregularly, sparsely and asynchronously sampled measurements of physiologic observations

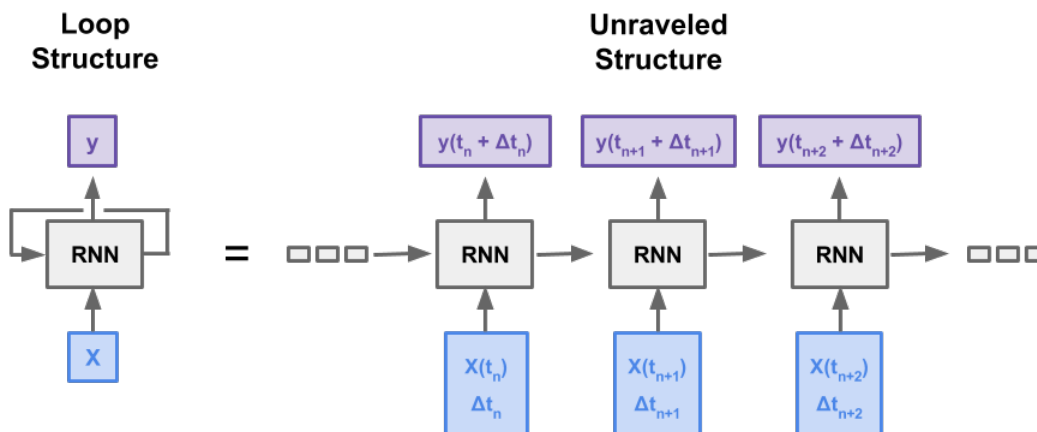


Figure 1: Flow of data in RNN-based framework. When measurements (vector X) become available at time t_n , they are ingested as inputs to the RNN kernel. The RNN then generates a prediction Y corresponding to a future time specified by the user through Δt_n .

(e.g. heart rate, blood pressure), laboratory results (e.g. creatine, glucose level), drugs (e.g. epinephrine, furosemide) and interventions (e.g. intubation, oxygen level).

A single patient can have multiple encounters, and this is an important point for validation. When the database was split into training and testing sets, all encounters from a single patient belonged to exactly one of these sets to prevent possible leakage. Encounters that did not include disposition information were excluded from the final database used for the results presented here. This database consisted of 12020 patients with 16559 encounters. Seventy-five percent of the patients were randomly selected and placed into the training set, and the remaining twenty-five percent into a holdout set for testing. This splitting resulted in 12460 encounters (with 4.85% mortality) in the training set, and 4099 encounters (with 5.12% mortality) in the holdout set.

To leverage existing deep learning frameworks, the data were first converted into the matrix format illustrated in Figure 2 with a pre-processing pipeline described below.

2.1 Constituent Aggregation and Normalization

Similar physiologic observations or laboratory measurements were aggregated into a single variable. For example, non-invasive and invasive measurements of systolic blood pressures were grouped together into a single systolic blood pressure variable. This aggregation resulted in approximately 300 different physiologic and treatment variables, a complete list of which can be found in Appendix A.

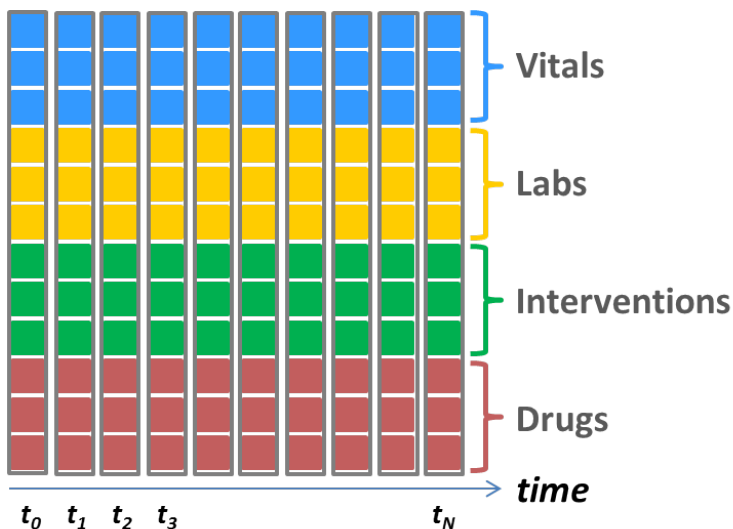


Figure 2: After pre-processing, data for a single patient encounter is in a matrix format. A single row of data contains values (actual and imputed measurements) from a single variable. A column of data comprises all measurements at one time point.

All quantities under the same variable were converted into the same unit of measure. Drugs and some interventions were converted to a binary variables corresponding to absence or presence of administration. Variables that were not binarized were Z-normalized. The mean and standard deviation needed for this transformation were computed from the training set only, and then applied to both the training and holdout sets.

2.2 Imputation

The measurements in the database were *sparse, irregularly sampled* – time between any two consecutive time points ranges from a minute to several hours – and *asynchronous*. At any time point when at least one variable had a recorded value, the values for all other variables without a measurement at that point were imputed. The imputation process depended on the variable type. Any missing measurement of a drug or an intervention variable was imputed as zero. When a physiologic observation or lab measurement was available, it was propagated forward until its next reading. However, if a physiologic or laboratory variable had no recorded value throughout the entire encounter, then that variable was set to zero at all time points for that encounter. Since physiologic observations were first Z-normalized, a zero imputation is equivalent to an imputation with the population mean derived from the training set. Note that no features were age-normalized; instead age was an input as a physiologic observation. These choices were based on a reasonable assumption about clinical practice: measurements are taken more frequently when *something* is happening to the patient, and less frequently when the patient appears *stable*.

3. RNN-based Framework

3.1 From dynamical system to RNN

The trajectory of a patient can be viewed as a continuous dynamical system composed of many variables, $P(t) = [\text{vitals, labs, drugs, interventions}]^T$, interacting with each other:

$$\frac{dP(t)}{dt} = F[P(t)], \quad P(t_0) = P_0. \tag{1}$$

In equation (1), F denotes the unknown and complex function governing the variable interactions, while P_0 is the state at some initial time, t_0 . For the PICU setting and data, t_0 corresponds to the start time of an ICU encounter.

Finite difference methods are a standard way to solve equation (1) [LeVeque (2007)]. Any such approximation can be cast into the form

$$P(t_n + \Delta t_n) = G[P(t_n), \Delta t_n, P(t_{n-1}), \dots, P(t_{n-k})], \tag{2}$$

where $t_n + \Delta t_n$ is a specified future time of interest. This can be further abstracted into the form:

$$P(t_n + \Delta t_n) = G\left[P(t_n), \Delta t_n, H[P(t_{n-1}), \dots, P(t_{n-k})]\right], \tag{3}$$

where H is a transformation of data from previous time steps. Equation (3) – which can be visualized in Figure 3 – is a recurrent relation, and G describes the mapping from past states into a future state.

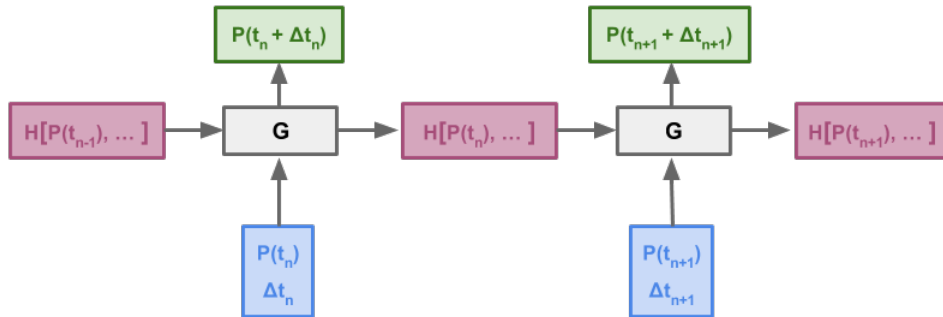


Figure 3: Visual diagram of finite difference formulation given in Equation 3.

Independent work by Funahashi (1989) and Hornik et al. (1989) established that any function with mathematically reasonable properties can be approximated by a neural net-

work to an arbitrary degree of accuracy, i.e.

$$G = \underbrace{\sum_i \alpha_i \sigma \left[W_i \left(P(t_n), \Delta t_n, H[P(t_{n-1}), \dots, P(t_{n-k})] \right) + b_i \right]}_{\text{Neural Network: } N} + \epsilon, \quad (4)$$

where ϵ is an arbitrarily small real number. The finite difference formulation therefore becomes

$$P(t_n + \Delta t_n) \approx N \left[P(t_n), \Delta t_n, H[P(t_{n-1}), \dots, P(t_{n-k})] \right]. \quad (5)$$

The output of H can be regarded as a *hidden state* or an internal representation of the patient’s history, and the mortality risk can be inferred from this integration of history. The diagram of Figure 3 then leads to the RNN formulation shown in Figure 4, where the RNN module encapsulates G from Equation (2) and an additional function that transforms the internal state to some observable manifestation, such as mortality risk, represented by the output y . The recurrent aspect of the network, i.e. the feedback mechanism, allows past information to be propagated forward.

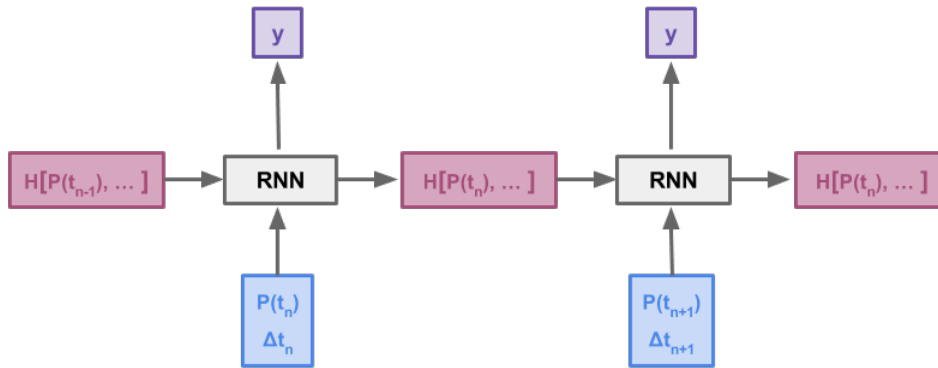


Figure 4: The output of the RNN, y , is another transformation

It is worth noting that work by Funahashi and Nakamura (1993) showed a direct path from dynamical systems to a class of continuous time recurrent neural networks (CTRNN) provided the original function, F , in Equation (1) meets continuity conditions. Chow and Li (2000) and Li et al. (2005) extended the theory to handle more general dynamical systems, including time-variant ones with inputs for control. Applying a finite difference scheme to the CTRNN leads to a form that is very similar to Equation (5).

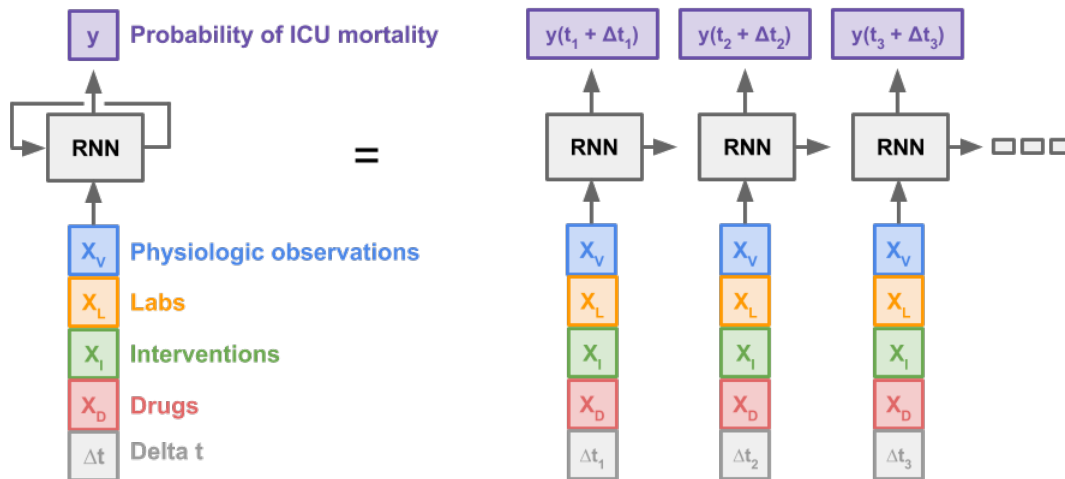


Figure 5: Physiologic observations, laboratory measurements, interventions and drugs at time t_n are inputs to the RNN kernel. The RNN then projects a mortality risk for time $t_n + \Delta t_n$, where Δt_n is specified by a user.

3.2 RNN architecture and implementation

Figure 5 illustrates the flow of the PICU data and predictions in the RNN-based infrastructure. The input vector to the network at time t_n consists of five main groups of measurements from a patient’s ICU encounter: $[X_V(t_n), X_L(t_n), X_I(t_n), X_D(t_n), \Delta t_n]^T$. The vector X_V contains the physiologic observations, the vector X_L contains laboratory results, the vector X_I comprises the interventions, X_D records the administered drugs, and the scalar Δt_n specifies how far into the future the user wants to forecast. Including Δt_n in the input vector follows naturally from the finite difference formulation (2) and serves a dual purpose: it gives the user control and flexibility in time-to-prediction, and it also enables augmentation of the training data during model development. The output at this time step is a probability of survival at the future time $t_n + \Delta t_n$ which can be thought of as a prediction of patient condition at that future time.

A number of RNN architectures have been developed and studied (Greff et al., 2015; Jozefowicz et al., 2015). The specific one utilized here is the Long Short-Term Memory (LSTM) architecture of Hochreiter and Schmidhuber (1997). The Keras python deep learning framework (Chollet, 2015) was used to construct a model comprised of three LSTMs – see Figure 6 – and train this model to make predictions for in-ICU mortality.

4. Results

The RNN model continuously updates its mortality risk predictions as it intakes new data. Figure 7 displays these temporally evolving risk scores from two patients. This dynamic

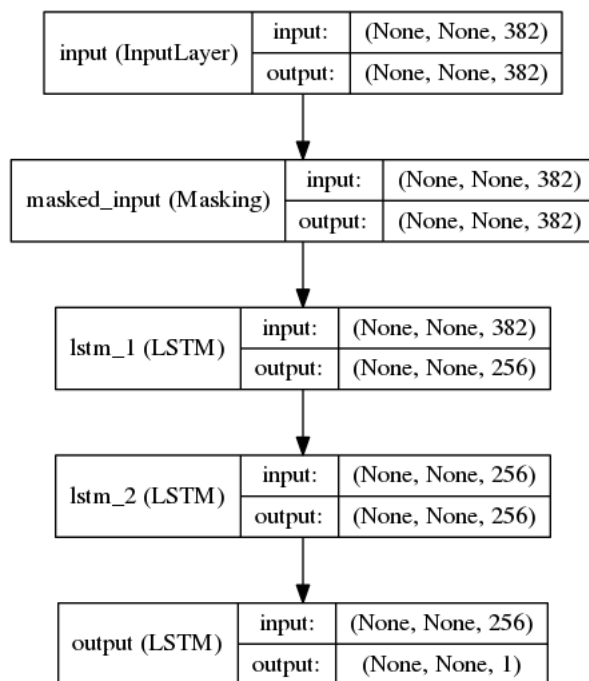


Figure 6: RNN architecture for PICU data

tracking, which is automatic in the RNN, is not done by PIM 2 or PRISM 3. The Rothman index updates its predictions when new measurements become available, but its update does not integrate past measurements. In this sense, the Rothman index still processes time series data in a static manner, while the RNN dynamically integrates data through its feedback mechanism.

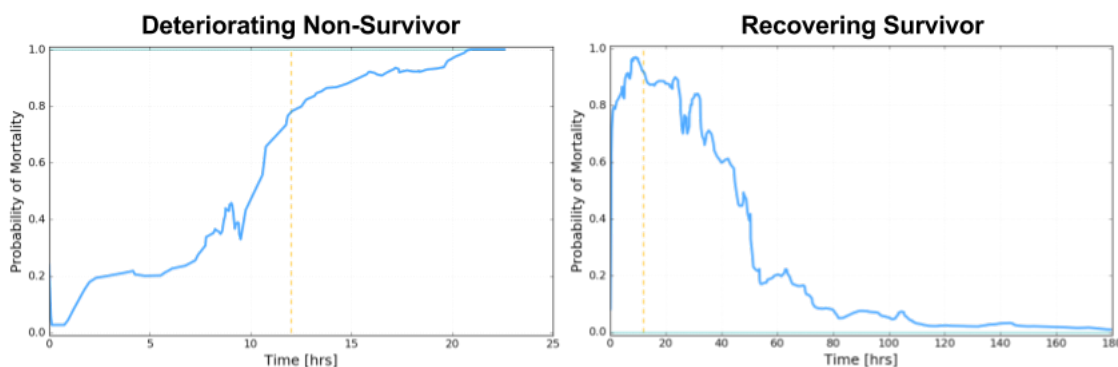


Figure 7: RNN-generated mortality risk of two patients tracked over their ICU encounter. The dashed yellow lines indicate the 12-hour mark. The patient on the left slowly deteriorated over the course of a day and did not survive. The patient on the right started as very high-risk but recovered over the course of a week.

The RNN’s ICU mortality predictions were compared to those of PIM 2 and PRISM 3, both of which were pulled directly from the EMR. A logistic regression (LR) and a multi-layer perceptron (MLP) were also implemented for additional comparisons. The LR, MLP and RNN models access identical clinical data. Like PIM 2 and PRISM 3, LR and MLP are *static* methods, meaning they process a snapshot of data from a fixed window of time to make a single-time prediction. Again, this is a contrast to the RNN which continuously integrates incoming data with past information. Both PIM 2 and PRISM 3 use information collected prior to ICU admission, data which the RNN, MLP and LR models do not access. In addition, PIM 2 incorporates some data from the first hour in the ICU, while PRISM 3 uses data from the first 12 hours in the ICU.

The ICU mortality predictions of the different models were assessed via Receiver Operating Characteristic (ROC) curves and corresponding Area Under the Curve (AUC). Figure 8 shows the results on 2849 holdout encounters that had both PIM 2 and PRISM 3 scores. The RNN model yields an AUC of 93.4% which is significantly higher than the comparative models [MLP: 88.8% ($p < 0.01$), LR: 86.1% ($p < 0.001$), PIM 2: 86.3% ($p < 0.001$), and PRISM 3: 88.0% ($p < 0.003$)]. The LR, MLP and RNN predictions used to generate these results were all taken from the 12th hour. The difference in performance between the MLP and RNN provides a rough quantification of the boost that dynamic integration provides over static computation. The feedback loop gives the RNN a temporal memory which enables temporal trends – i.e., function derivatives – to be incorporated into the model.

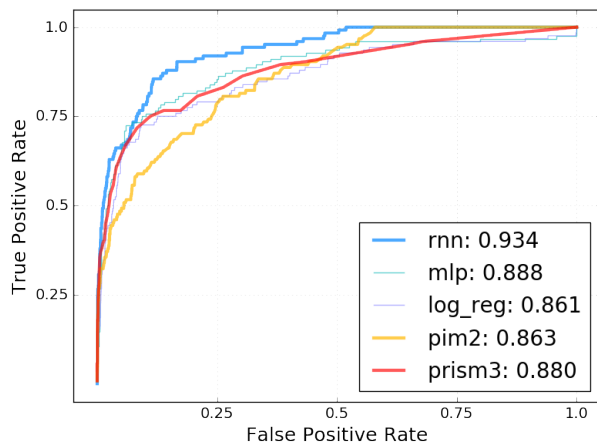


Figure 8: Comparison of ICU mortality predictions from various models: Recurrent Neural Network, Multi-Layer Perceptron, Logistic Regression, PIM2, and PRISM3. ROC curves and AUCs were generated from 2849 holdout encounters that had both PIM 2 and PRISM 3 scores available.

Figure 9 demonstrates the improved predictive capability of the RNN model as a function of increasing observation time. After only three hours of observation, the RNN’s AUC surpasses that of PRISM 3 which incorporates 12 hours of observation. As the RNN’s observation window increases, the accuracy of its prediction continues to increase. This is a desirable characteristic of a risk score.

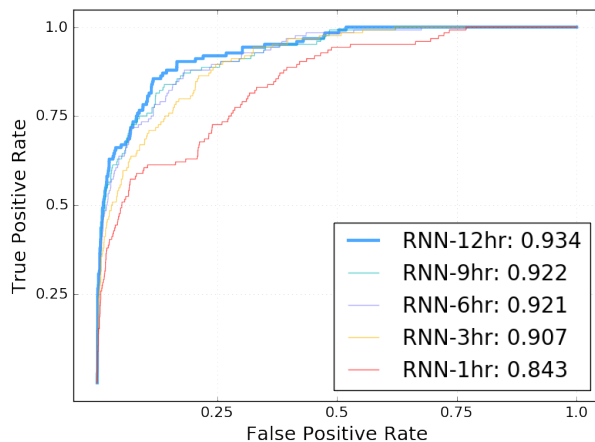


Figure 9: Comparison of ICU mortality predictions from RNN model after various lengths of observation time. These results were aggregated from the same 2849 holdout encounters in the previous figure. All had least 12 hours of data.

5. Conclusions

Recurrent Neural Networks were applied on ICU EMR to generate in-ICU mortality risk scores. In addition to providing dynamic tracking of patient condition, the RNN-generated scores also achieved significantly higher accuracy [AUROC greater than 93%] than the clinically used systems PIM 2 and PRISM 3. The RNN model also outperformed logistic regression and multi-layer perceptron models. The increased performance of the RNN model stemmed from two key factors: access to more variables that characterize a patient and dynamic integration that allows it to incorporate temporal trends of those variables.

Although approximately 300 variables have been encoded into the model, other data which are available from the PICU, such as fluid balance, have not been incorporated. Monitor data, which have higher temporal resolution, also have yet to be included. Future work will focus on aggregating these additional data and quantifying their impact on predictive accuracy.

Acknowledgments

This work was funded by a grant from the Laura P. and Leland K. Whittier Foundation.

References

Ahmed M Alaa, Jinsung Yoon, Scott Hu, and Mihaela van der Schaar. Personalized risk scoring for critical care patients using mixtures of gaussian process experts. *arXiv preprint arXiv:1605.00959*, 2016.

F Chollet. Keras. <https://github.com/fchollet/keras>, 2015.

Tommy WS Chow and Xiao-Dong Li. Modeling of continuous time dynamical systems with input by recurrent neural networks. *IEEE Transactions on Circuits and Systems I*:

- Fundamental Theory and Applications*, 47(4):575–578, 2000.
- Ken-Ichi Funahashi. On the approximate realization of continuous mappings by neural networks. *Neural networks*, 2(3):183–192, 1989.
- Ken-ichi Funahashi and Yuichi Nakamura. Approximation of dynamical systems by continuous time recurrent neural networks. *Neural networks*, 6(6):801–806, 1993.
- Marzyeh Ghassemi, Marco AF Pimentel, Tristan Naumann, Thomas Brennan, David A Clifton, Peter Szolovits, and Mengling Feng. A multivariate timeseries modeling approach to severity of illness assessment and forecasting in icu with sparse, heterogeneous clinical data. In *AAAI*, pages 446–453, 2015.
- Klaus Greff, Rupesh Kumar Srivastava, Jan Koutník, Bas R Steunebrink, and Jürgen Schmidhuber. Lstm: A search space odyssey. *arXiv preprint arXiv:1503.04069*, 2015.
- C William Hanson III and Bryan E Marshall. Artificial intelligence applications in the intensive care unit. *Critical care medicine*, 29(2):427–435, 2001.
- Kaiming He, Xiangyu Zhang, Shaoqing Ren, and Jian Sun. Deep residual learning for image recognition. *arXiv preprint arXiv:1512.03385*, 2015.
- Geoffrey Hinton, Li Deng, Dong Yu, George E Dahl, Abdel-rahman Mohamed, Navdeep Jaitly, Andrew Senior, Vincent Vanhoucke, Patrick Nguyen, Tara N Sainath, et al. Deep neural networks for acoustic modeling in speech recognition: The shared views of four research groups. *IEEE Signal Processing Magazine*, 29(6):82–97, 2012.
- Sepp Hochreiter and Jürgen Schmidhuber. Long short-term memory. *Neural computation*, 9(8):1735–1780, 1997.
- Kurt Hornik, Maxwell Stinchcombe, and Halbert White. Multilayer feedforward networks are universal approximators. *Neural networks*, 2(5):359–366, 1989.
- Rafal Jozefowicz, Wojciech Zaremba, and Ilya Sutskever. An empirical exploration of recurrent network architectures. In *Proceedings of the 32nd International Conference on Machine Learning (ICML-15)*, pages 2342–2350, 2015.
- William A Knaus, Elizabeth A Draper, Douglas P Wagner, and Jack E Zimmerman. Apache ii: a severity of disease classification system. *Critical care medicine*, 13(10):818–829, 1985.
- William A Knaus, Douglas P Wagner, Elizabeth A Draper, Jack E Zimmerman, Marilyn Bergner, Paulo G Bastos, Carl A Sirio, Donald J Murphy, Ted Lotring, and Anne Damiano. The apache iii prognostic system. risk prediction of hospital mortality for critically ill hospitalized adults. *Chest Journal*, 100(6):1619–1636, 1991.
- Alex Krizhevsky, Ilya Sutskever, and Geoffrey E Hinton. Imagenet classification with deep convolutional neural networks. In *Advances in neural information processing systems*, pages 1097–1105, 2012.
- Jean-Roger Le Gall. The use of severity scores in the intensive care unit. *Intensive care medicine*, 31(12):1618–1623, 2005.

- Jean-Roger Le Gall, Philippe Loirat, Annick Alperovitch, Paul Glaser, Claude Granthil, Daniel Mathieu, Philippe Mercier, Remi Thomas, and Daniel Villers. A simplified acute physiology score for icu patients. *Critical care medicine*, 12(11):975–977, 1984.
- Randall J LeVeque. *Finite difference methods for ordinary and partial differential equations: steady-state and time-dependent problems*, volume 98. Siam, 2007.
- Xiao-Dong Li, John KL Ho, and Tommy WS Chow. Approximation of dynamical time-variant systems by continuous-time recurrent neural networks. *IEEE Transactions on Circuits and Systems II: Express Briefs*, 52(10):656–660, 2005.
- Grégoire Mesnil, Yann Dauphin, Kaisheng Yao, Yoshua Bengio, Li Deng, Dilek Hakkani-Tur, Xiaodong He, Larry Heck, Gokhan Tur, Dong Yu, et al. Using recurrent neural networks for slot filling in spoken language understanding. *IEEE/ACM Transactions on Audio, Speech and Language Processing (TASLP)*, 23(3):530–539, 2015.
- Rui P Moreno, Philipp GH Metnitz, Eduardo Almeida, Barbara Jordan, Peter Bauer, Ricardo Abizanda Campos, Gaetano Iapichino, David Edbrooke, Maurizia Capuzzo, Jean-Roger Le Gall, et al. Saps 3 from evaluation of the patient to evaluation of the intensive care unit. part 2: Development of a prognostic model for hospital mortality at icu admission. *Intensive care medicine*, 31(10):1345–1355, 2005.
- Murray M Pollack. Severity of illness confusion. *Pediatric Critical Care Medicine*, 17(6):583, 2016.
- Murray M Pollack, Urs E Ruttimann, and Pamela R Getson. Pediatric risk of mortality (prism) score. *Critical care medicine*, 16(11):1110–1116, 1988.
- Murray M Pollack, Kantilal M Patel, and Urs E Ruttimann. Prism iii: an updated pediatric risk of mortality score. *Critical care medicine*, 24(5):743–752, 1996.
- Murray M Pollack, Richard Holubkov, Tomohiko Funai, J Michael Dean, John T Berger, David L Wessel, Kathleen Meert, Robert A Berg, Christopher JL Newth, Rick E Harrison, et al. The pediatric risk of mortality score: update 2015. *Pediatric Critical Care Medicine*, 17(1):2–9, 2016.
- Michael J Rothman, Steven I Rothman, and Joseph Beals. Development and validation of a continuous measure of patient condition using the electronic medical record. *Journal of biomedical informatics*, 46(5):837–848, 2013.
- F Shann, G Pearson, A Slater, and K Wilkinson. Paediatric index of mortality (pim): a mortality prediction model for children in intensive care. *Intensive care medicine*, 23(2):201–207, 1997.
- Anthony Slater, Frank Shann, Gale Pearson, PIM Study Group, et al. Pim2: a revised version of the paediatric index of mortality. *Intensive care medicine*, 29(2):278–285, 2003.
- K Strand and H Flaatten. Severity scoring in the icu: a review. *Acta Anaesthesiologica Scandinavica*, 52(4):467–478, 2008.

Lahn Straney, Archie Clements, Roger C Parslow, Gale Pearson, Frank Shann, Jan Alexander, Anthony Slater, ANZICS Paediatric Study Group, the Paediatric Intensive Care Audit Network, et al. Paediatric index of mortality 3: an updated model for predicting mortality in pediatric intensive care. *Pediatric Critical Care Medicine*, 14(7):673–681, 2013.

Appendix A. Clinical Data Used

Vitals	
Abdominal girth	Bladder pressure
Capillary refill rate	Central Venous Pressure
Cerebral perfusion pressure	Diastolic Blood Pressure
EtCO ₂	Eye Response
GlascowCS	Head circumference
Heart rate	Height
Intracranial pressure	Left pupillary response
Motor Response	Near-infrared spectroscopy %
Pulse Oximetry	Pupillary response
Respiratory rate	Right pupillary response
Systolic Blood Pressure	Temperature
Verbal Response	Weight

Labs	
ABG Base excess	ABG FiO ₂
ABG HCO ₃	ABG O ₂ sat %
ABG PCO ₂	ABG PO ₂
ABG TCO ₂	ABG pH
ALT (SGPT)	AST (SGOT)
Albumin level	Alkaline phosphatase
Amylase	B-type Natriuretic Peptide
BUN	Bands %
Basophils %	Bicarbonate serum
Bilirubin conjugated	Bilirubin total
Bilirubin unconjugated	Blasts %
C-reactive protein	CBG Base excess
CBG FiO ₂	CBG HCO ₃
CBG O ₂ sat %	CBG PCO ₂
CBG PO ₂	CBG TCO ₂
CBG pH	CSF Bands %
CSF Lymphs %	CSF RBC
CSF Segs %	CSF WBC
CSF glucose	CSF protein
Calcium ionized	Calcium total
Chloride	Complement C3 serum
Complement C4 serum	Creatinine
Culture CSF	Culture blood
Culture fungus blood	Culture respiratory
Culture urine	Culture wound
ESR	Eosinophils %
FDP Titer	Ferritin level
Fibrinogen	GGT
Glucose	Haptoglobin

DYNAMIC MORTALITY RISK PREDICTION

Labs (cont.)

Hema	Hemo
INR	Lactate
Lactate Dehydrogenase blood	Lactic Acid blood
Lipase	Lymphocyte %
MCH	MCHC %
MCV	MVBG Base excess
MVBG FiO2	MVBG HCO3
MVBG O2 sat %	MVBG PCO2
MVBG PO2	MVBG TCO2
MVBG pH	Macrocytes
Magnesium level	Metamyelocytes %
Monocytes %	Myelocytes %
Neutrophils %	Oxygentaion index
P/F ratio	PT
PTT	PaO2/FiO2
Phosphorus level	Platelet count
Potassium	Protein total
RBC blood	RDW %
Reticulocyte count %	Schistocytes
Sodium	T4 free
TSH	Triglycerides
VBG Base excess	VBG FiO2
VBG HCO3	VBG O2 sat %
VBG PCO2	VBG PO2
VBG TCO2	VBG pH
Virus	White blood cell count

Interventions

Abdominal X ray	Alprostadil
Amplitude	CT abdomen
CT abdomen/pelvis	CT brain
CT chest	CT pelvis
Chest X ray	Chest/abd X ray
Continuous EEG	ECMO hours
ECMO type	EPAP
FiO2	Foley catheter
Frequency	Hemofiltration/CRRT
IPAP	Inspiratory time
MAP	MRI brain
Mean airway pressure	NIV set rate
Nitric Oxide	O2 Flow
PEEP	PEEP
Peak Inspiratory Pressure	Peritoneal dialysis
Pressure support	Tidal volume delivered

Interventions (cont.)

Tidal volume expiratory	Tidal volume inspiratory
Tidal volume set	Tracheostomy
Ventilator rate	Ventricular assist device
Volume Tidal	

Drugs

Acetaminophen	Acetaminophen/Codeine
Acetaminophen/Hydrocodone	Acetaminophen/Oxycodone
Acetazolamide	Acetylcysteine
Acyclovir	Albumin
Albuterol	Allopurinol
Alteplase	Amikacin
Aminocaproic Acid	Aminophylline
Amiodarone	Amlodipine
Amoxicillin	Amoxicillin/clavulanic acid
Amphotericin B	Amphotericin B Lipid Complex
Ampicillin	Ampicillin/Sulbactam
Aspirin	Atenolol
Atropine	Azathioprine
Azithromycin	Baclofen
Basiliximab	Budesonide
Bumetanide	Calcium Chloride
Calcium Glubionate	Calcium Gluconate
Captopril	Carbamazepine
Carvedilol	Caspofungin
Cefazolin	Cefepime
Cefotaxime	Cefoxitin
Ceftazidime	Ceftriaxone
Cefuroxime	Cephalexin
Chloral Hydrate	Chlorothiazide
Ciprofloxacin HCL	Cisatracurium
Clarithromycin	Clindamycin
Clonazepam	Clonidine HCl
Clotrimazole	Cromolyn Sodium
Cyclophosphamide	Cyclosporine
Dantrolene Sodium	Desmopressin
Dexamethasone	Dexmedetomidine
Diazepam	Digoxin
Diphenhydramine HCl	Dobutamine
Dopamine	Dornase Alfa
Doxacurium Chloride	Doxorubicin
Doxycycline Hyclate	Enalapril
Enoxaparin	Epinephrine
Epoetin	Erythromycin

DYNAMIC MORTALITY RISK PREDICTION

Drugs (cont.)

Esmolol Hydrochloride	Etomidate
Factor VII	Famotidine
Fentanyl	Ferrous Sulfate
Filgrastim	Flecainide Acetate
Fluconazole	Fluticasone
Fosphenytoin	Furosemide
Gabapentin	Ganciclovir Sodium
Gentamicin	Glycopyrrolate
Haloperidol	Heparin
Hydrocortisone	Hydromorphone
Ibuprofen	Imipenem
Immune Globulin	Insulin
Ipratropium Bromide	Isoniazid
Isoproterenol	Isradipine
Itraconazole	Ketamine
Ketorolac	Labetalol
Lactobacillus	Lansoprazole
Levalbuterol	Levetiracetam
Levocarnitine	Levofloxacin
Levothyroxine Sodium	Lidocaine
Linezolid	Lisinopril
Lorazepam	Magnesium Sulfate
Meropenem	Methadone
Methylprednisolone	Metoclopramide
Metolazone	Metronidazole
Micafungin	Midazolam HCl
Milrinone	Montelukast Sodium
Morphine	Mycophenolate Mofetil
Naloxone HCL	Naproxen
Nesiritide	Nifedipine
Nitrofurantoin	Nitroglycerine
Nitroprusside	Norepinephrine
Nystatin	Octreotide Acetate
Olanzapine	Ondansetron
Oseltamivir	Oxacillin
Oxcarbazepine	Oxycodone
Pancuronium	Pantoprazole
Penicillin G Sodium	Pentobarbital
Phenobarbital	Phenylephrine HCl
Phenytoin	Piperacillin
Piperacillin/Tazobactam	Potassium Chloride
Potassium Phosphate	Prednisolone
Prednisone	Procainamide
Propofol	Propranolol HCl

Drugs (cont.)

Prostacyclin	Protamine
Racemic Epi	Ranitidine
Rifampin	Risperidone
Rocuronium	Sildenafil
Sodium Bicarbonate	Sodium Chloride
Sodium Phosphate	Spirolactone
Sucalfate	Tacrolimus
Terbutaline	Theophylline
Ticarcillin	Ticarcillin/clavulanic acid
Tobramycin	Topiramate
Treprostinil	Trimethoprim/Sulfamethoxazole
Tromethamine	Ursodiol
Valganciclovir	Valproic Acid
Vancomycin	Vasopressin
Vecuronium	Vitamin E
Vitamin K	Voriconazole
Warfarin Sodium	